NANO LETTERS

Letter

pubs.acs.org/NanoLett

Connecting Dopant Bond Type with Electronic Structure in N-Doped Graphene

Theanne Schiros,*[,†] Dennis Nordlund,[‡] Lucia Pálová,[§] Deborah Prezzi,[∥] Liuyan Zhao,[⊥] Keun Soo Kim,[¶] Ulrich Wurstbauer,[⊥] Christopher Gutiérrez,[⊥] Dean Delongchamp,[■] Cherno Jaye,[●] Daniel Fischer,[▲] Hirohito Ogasawara,[‡] Lars G. M. Pettersson,[▼] David R. Reichman,[§] Philip Kim,[⊥] Mark S. Hybertsen,[⬢] and Abhay N. Pasupathy*[,⊥]

[†]Energy Frontier Research Center, Columbia University, New York, New York 10027, United States

[‡]Stanford Synchrotron Radiation Lightsource, Stanford Linear Accelerator Center, Menlo Park, California 94025, United States

[§]Department of Chemistry, Columbia University, New York, New York 10027, United States

[∥]S3 Center, CNR-Nanoscience Institute, I-41125 Modena, Italy

[⊥]Department of Physics, Columbia University, New York, New York 10027, United States

[¶]Department of Physics and Graphene Research Institute, Sejong University, Seoul 143-747, Korea

[■]Polymers Division, [●]Materials Measurement Laboratory, and [▲]Ceramics Division, National Institute of Standards and Technology, Gaithersburg, Maryland 20899, United States

[▼]Department of Physics, Stockholm University, S-106 91 Stockholm, Sweden

[⬢]Center for Functional Nanomaterials, Brookhaven National Laboratory, Upton, New York 11973-5000, United States

S *Supporting Information*

ABSTRACT: Robust methods to tune the unique electronic properties of graphene by chemical modification are in great demand due to the potential of the two dimensional material to impact a range of device applications. Here we show that carbon and nitrogen core-level resonant X-ray spectroscopy is a sensitive probe of chemical bonding and electronic structure of chemical dopants introduced in single-sheet graphene films. In conjunction with density functional theory based calculations, we are able to obtain a detailed picture of bond types and electronic structure in graphene doped with nitrogen at the sub-percent level. We show that different N-bond types, including graphitic, pyridinic, and nitrilic, can exist in a single, dilutely N-doped graphene sheet. We show that these various bond types have profoundly different effects on the carrier concentration, indicating that control over the dopant bond type is a crucial requirement in advancing graphene electronics.

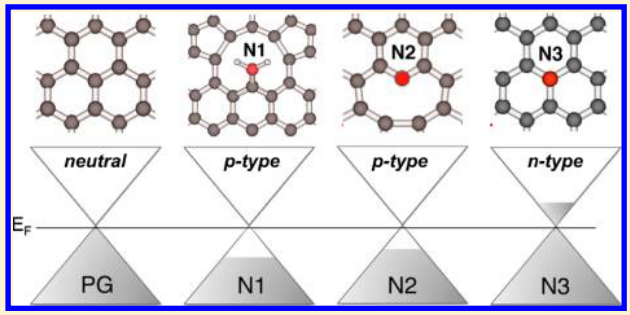

KEYWORDS: *Nitrogen-doped graphene, workfunction, bonding, electronic structure, X-ray spectroscopy*

The two dimensional (2D) nature of graphene endows it with a number of unique properties that make it a promising electronic contact material, including high conductivity ($R \sim 20-30$ Ohm/square), transparency,[1] and tunable electron density.[2,3] The opportunity to tune the work function and carrier concentration of graphene enables a range of electronic and optical applications,[4] and diverse methods to achieve this are being actively explored. Electrostatic gating is one well-established method,[3] but chemical modification on graphene's basal plane can potentially achieve the required control without the use of external voltages. Several recent experiments have explored chemical modification of graphene with foreign atoms including nitrogen,[5−14] boron,[15,16] fluorine,[17] and hydrogen.[18] In general, these atomic dopants can be incorporated via several different bond types in a graphene sheet. A microscopic understanding of the different bond types and their diverse effects on the workfunction, carrier concentration, and the local electronic structure in nitrogen-doped graphene films is therefore highly desirable.

The high energy resolution and tunable polarization and energy of synchrotron light enable the detection of chemically distinct species and the identification of bond types even of sub-percent level dopants in monolayer graphene. Recent scanning tunneling microscopy (STM) and spectroscopy measurements have provided important information on the electronic structure of the films near the Fermi energy.[13]

Received: April 14, 2012
Revised: June 27, 2012
Published: June 29, 2012

Report Documentation Page

Form Approved
OMB No. 0704-0188

1. REPORT DATE	2. REPORT TYPE	3. DATES COVERED
29 JUN 2012		**00-00-2012 to 00-00-2012**

4. TITLE AND SUBTITLE	5a. CONTRACT NUMBER
Connecting Dopant Bond Type with Electronic Structure in N-Doped Graphene	5b. GRANT NUMBER
	5c. PROGRAM ELEMENT NUMBER
6. AUTHOR(S)	5d. PROJECT NUMBER
	5e. TASK NUMBER
	5f. WORK UNIT NUMBER
7. PERFORMING ORGANIZATION NAME(S) AND ADDRESS(ES) **Columbia University,Energy Frontier Research Center,New York,NY,10027**	8. PERFORMING ORGANIZATION REPORT NUMBER
9. SPONSORING/MONITORING AGENCY NAME(S) AND ADDRESS(ES)	10. SPONSOR/MONITOR'S ACRONYM(S)
	11. SPONSOR/MONITOR'S REPORT NUMBER(S)

12. DISTRIBUTION/AVAILABILITY STATEMENT
Approved for public release; distribution unlimited

13. SUPPLEMENTARY NOTES

14. ABSTRACT

Robust methods to tune the unique electronic properties of graphene by chemical modification are in great demand due to the potential of the two dimensional material to impact a range of device applications. Here we show that carbon and nitrogen core-level resonant X-ray spectroscopy is a sensitive probe of chemical bonding and electronic structure of chemical dopants introduced in single-sheet graphene films. In conjunction with density functional theory based calculations, we are able to obtain a detailed picture of bond types and electronic structure in graphene doped with nitrogen at the sub-percent level. We show that different N-bond types, including graphitic, pyridinic, and nitrilic, can exist in a single, dilutely N-doped graphene sheet. We show that these various bond types have profoundly different effects on the carrier concentration, indicating that control over the dopant bond type is a crucial requirement in advancing graphene electronics.

15. SUBJECT TERMS

16. SECURITY CLASSIFICATION OF:			17. LIMITATION OF ABSTRACT	18. NUMBER OF PAGES	19a. NAME OF RESPONSIBLE PERSON
a. REPORT **unclassified**	b. ABSTRACT **unclassified**	c. THIS PAGE **unclassified**	**Same as Report (SAR)**	**7**	

However, STM is restricted to low (<1 V) energy measurements so that information on the energy and symmetry of the valence orbitals and the chemical bond environments of atoms is limited. Here we use photoelectron (XPS) spectroscopy, carbon and nitrogen core-level X-ray absorption (XAS) and emission (XES) spectroscopy in combination with density functional theory (DFT) based calculations to obtain an atom-specific picture of dilutely doped, single-layer graphene (SLG), despite the small probability of radiative core hole decay and the weak signal from subpercent atomic dopant levels. XAS provides direct information on the dopant bond type, orientation, and concentration. Coupling XAS, which probes the local unoccupied density of states for a given atom of interest, with XES, which provides complementary atom-specific and symmetry-resolved information about the local occupied density of states, allows us to identify the influence of different N-dopants on the graphene electronic structure.

Figure 1 shows angle-dependent XAS measured in total electron yield (TEY) mode at the carbon and nitrogen K-edges

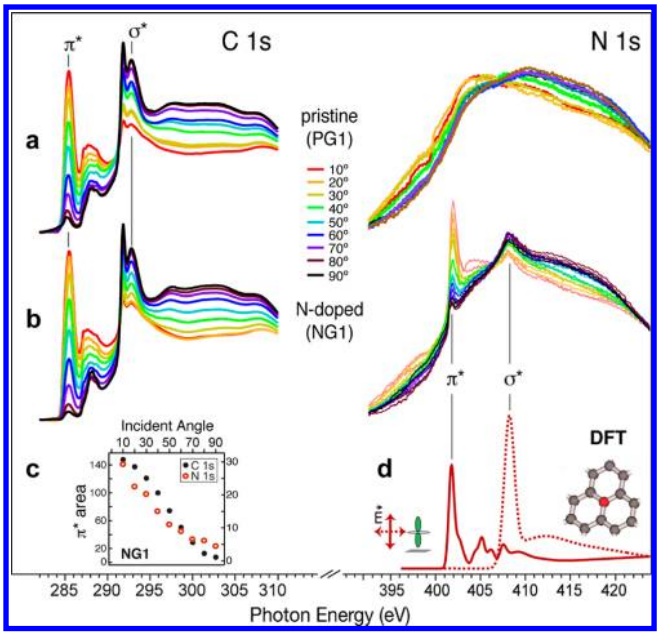

Figure 1. C 1s (left) and N 1s (right) XAS measurements for (a) pristine and (b) N-doped graphene (grown) on Cu foil. (c) Strong dependence of the integrated XAS intensity (area) of the π^* resonance on incident angle, which is largest when the E-vector of the light is out-of-plane (grazing angle 10°), clearly shows the planar orientation of both the C=C and C=N bonds in the graphene lattice. (d) DFT-computed XAS for a substitutional nitrogen dopant bonded to three carbons (graphitic (N3)) in the graphene lattice; the match to experiment is clear.

for pristine (PG) and NH_3-grown graphene (NG1) on Cu foil (sample preparation details in the Supporting Information).[13] The C 1s XAS (left panel) shows the characteristic spectral signature of graphene, including strong peaks at ~285 and ~292 eV, corresponding, respectively, to the 1s to π^* and σ^* C=C bond resonances, as well as the sharp excitonic feature at 291.5 eV indicative of long-range order in the electronic structure of pristine graphene; these spectral features are also found in graphite.[18,20] The spectra display the strong angular dependence expected for the planar bonds of a 2D system.[19] The C 1s XAS is nearly identical for the pristine and N-doped graphene on Cu foil, indicating that the dilute nitrogen concentration in the doped sample does not disrupt the high quality of the graphene sheet. Importantly, such a disruption can be observed for higher ammonia concentrations during CVD growth, indicative of sample quality (Supporting Information Figure S2).

In the N 1s XAS (right panel), no distinct peaks appear in the pristine graphene spectra as expected. The N-doped sample shows sharp XAS peaks at ~401 and 408 eV, corresponding to 1s to π^* and σ^* transitions, respectively, for a single, well-defined substitution type. The angular dependence of the N 1s XAS follows that of the carbon XAS, indicating that the features are due to planar N−C bonds in the graphene sample (Figure 1b,d). On the basis of these two observations and previous studies on related systems, we assign the nitrogen species to sp^2-bonded graphitic nitrogen with three C neighbors.[21−24] For comparison, calculations based on DFT are used to probe spectral features for specific dopant structures[25,26] (details of the methods are provided in the Supporting Information including Figure S1). The excellent match of the computed XAS for the N3-dopant (Figure 1d) corroborates this assignment, establishing a clear spectral fingerprint of graphitic nitrogen.

XPS is the determinative analysis tool that provides information on atomic concentration and local coordination environment and has been applied to the study of N-doping in graphene.[5,9] Figure 2a shows the N 1s XPS for the same PG1 and NG1 samples on Cu foil shown in Figure 1, as well as for N-doped graphene (grown at a lower NH_3-partial pressure) transferred to SiO_2 (NG2/SiO_2). NG1 shows a weak, broad peak at ~400 eV binding energy (BE) that we unequivocally assign to graphitic (N3) dopants based on the XAS (Figure 1), which is in agreement with studies of modified carbon films.[22,27,28] Using tabulated photoelectron cross sections of nitrogen and carbon,[29] a total nitrogen concentration of ~0.4% is obtained for N-doped graphene on both the Cu foil and transferred to SiO_2.[30] In Figure 2c, individual N3 dopants are visualized for the NG1 sample using STM, observed as bright triangular spots. By simply counting bright spots in the image, we estimate ~0.3% substitutional nitrogen in the graphene lattice, which is in good agreement with the value obtained from XPS.

Whereas the nitrogen dopants in NG1 can be assigned to graphitic (N3) nitrogen, the asymmetric peak of the transferred sample NG2/SiO_2 (Figure 2a) indicates that (at least) two N−C bond species contribute to the total nitrogen concentration. We use N1, N2, and N3 to denote nitrogen with one (nitrile-like), two (pyridinic) and three (graphitic) carbon bonds, respectively. In addition to the N3 peak (~400 eV), the transferred NG2/SiO_2 sample also has intensity at lower BE (~398.5 eV), indicating less electronegative N−C bonds, that in previous studies have been assigned to pyridinic (N2)[21,31] and nitrilic (N1) groups.[21] However, the multitude of possible N-bond configurations (graphitic, pyridinic, pyrrolic, nitrilic) with similar BE and the broadness of the photoemission peaks make the identification of bond types difficult, as evidenced by the range of interpretations of similar data sets.[21,31−33]

We return to N 1s XAS to identify the origin(s) of the low BE feature in the N 1s photoemission. Figure 3 compares angle-dependent N 1s XAS measured in partial electron yield (PEY) mode for N-doped graphene grown on Cu foil (NGA, Figure 3a) and quickly loaded into UHV with samples transferred to SiO_2 (NGB/SiO_2, Figure 3b) or on Cu foil mechanically bent during brief exposure to ambient atmosphere

dx.doi.org/10.1021/nl301409h | Nano Lett. 2012, 12, 4025−4031

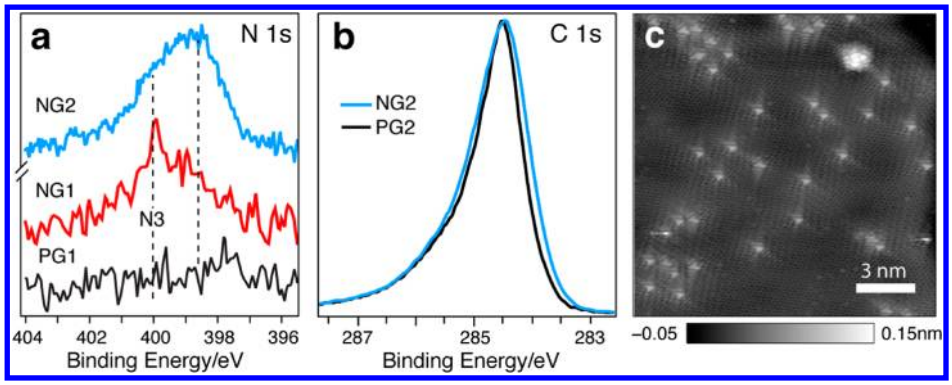

Figure 2. (a) N 1s and (b) C 1s XPS, for pristine (PG1) and N-doped graphene (NG1) samples grown on Cu foil and for samples transferred to SiO_2 (PG2(/SiO_2), NG2(/SiO_2)). XAS for samples PG1 and NG1 are shown in Figure 1. Quantitative XPS analysis is based on spectra normalized on the high kinetic energy side; the C 1s XPS shown here is normalized to maximum peak height to facilitate comparison of peak shape. (c) STM image showing individual graphitic dopants in sample NG1.

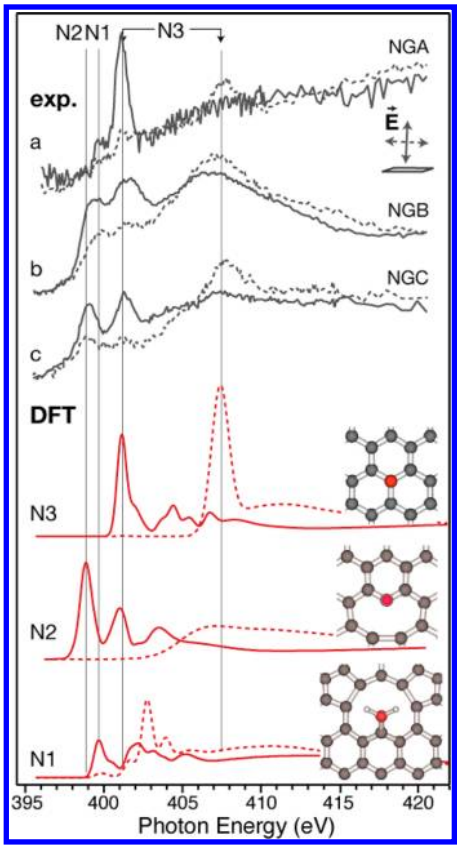

Figure 3. Experimental N 1s XAS (gray curves) measured in PEY mode for (a) NGA (on Cu); (b) NGB transferred to SiO_2; (c) NGC (on Cu) exposed to ambient atmosphere, and DFT-computed spectra (red curves) for cluster models of graphitic (N3); pyridinic (N2); and nitrile-like (N1(+H)) nitrogen dopants, used to assign the experimental resonances. Solid and dashed lines indicate out-of-plane and in-plane intensity, respectively, in the computed spectra; the measurements were taken at grazing incidence of 20° (solid line) and 70° (dashed line).

(NGC, Figure 3c) with the latter two showing a low BE component in addition to the graphitic (N3) peak (see Figure 2a). Because the XPS BE is referenced to the sample Fermi energy, for a metallic system such as graphene it can be directly correlated to the onset energy for the XAS (see, e.g., ref 34). Accordingly, new π^* resonances appear at lower photon energy (399 and 399.5 eV) for NGB (on SiO_2) and NGC (on Cu) in addition to the graphitic peak (NGA), each corresponding to a distinct N−C bond species (Figure 3 top). On the basis of DFT-computed spectra for different N-bond structures shown in the lower panel of Figure 3, we assign the peaks at 399 and 399.5 eV to pyridinic (N2) and hydrogenated N1-type dopants, respectively, which is in agreement with previous studies of modified carbon systems (Figure 3 inset).[21,24,31−33] In contrast to the sharp π^* and σ^* resonances of substitutionally N-doped graphene (NGA), NGB and NGC show a weaker, broader, and energy-shifted σ^* resonance as predicted by theory for N2 and N1 dopants (Figure 3b, bottom), which is also similar to the case of high NH_3 growth (Supporting Information Figure S2). (We note that the computed XAS spectrum and electronic structure effect of one pyridinic (N2) dopant at a vacancy site is very similar to the case of three such dopants (see Table 1); we show the case of a single N2 dopant here for simplicity.)

Table 1. Computed Work Function, Doping Effect, and Fraction of Electrons Added or Withdrawn (−) from the Lattice Per N-Dopant for the Different Bond Types Compared to Pristine Graphene (PG) and Graphene with Vacancy Defects

bond type	work function (eV)	doping effect	n_e/N
PG	4.43	−	−
vacancy	4.74	p	−
vacancy + H	4.71	p	−
graphitic (N3)	3.98	n	0.54
pyridinic (N2)	4.83	p	−0.45
pyridinic (+H)	4.29	n	0.02
nitrilic (N1)	4.92	p	−0.65
nitrilic (+H)	4.83	p	−0.66
nitrilic (+2H)	4.82	p	−0.48

How do the different N-bond environments affect the macroscopic electronic structure of doped graphene? With clear correlations between the spectroscopic signatures in Figures 1 and 3 and local dopant bonding motifs, DFT calculations for extended graphene sheets with 1% of the dopant structures[35] (details provided in the Supporting Information) are used to probe changes in the work function for the different N-bond environments and the fractional charge added (withdrawn) per N atom for each dopant type (Table 1). The different N-bond types have profoundly different macroscopic electronic structure effects on the graphene. We find that graphitic

dx.doi.org/10.1021/nl301409h | Nano Lett. 2012, 12, 4025−4031

nitrogen (N3) n-dopes graphene, consistent with the expected picture of substitutional N-doping.[13] In contrast, pyridinic (N2) and nitrile-like (N1, with or without H) dopants, which occur at vacancy sites and domain edges, and vacancy defects themselves, produce p-type doping of graphene. Table 1 shows that ~0.5 electron per N-dopant is added to the carbon π-network in the N3 case, which is in excellent agreement with scanning tunneling spectroscopy data.[13] On the other hand, pyridinic and nitrile-like nitrogen remove charge from graphene resulting in p-type doping and an increase of the work function, which was experimentally confirmed by measuring the workfunction of transferred graphene with various degrees of N2 and N1 dopants relative to pristine graphene (see Supporting Information Figure S3). This understanding, coupled with increasing control over N2/N3 ratios in N-doped graphene,[14] opens new avenues for tailoring the carrier density and electronic properties of graphene at the atomic level.

In the following, we show that core-level spectroscopy and DFT are sensitive to the details of the effect of the different dopant bond structures and vacancy defects on the electronic structure of graphene. The diverse effects on the carrier density in graphene are visualized in computed charge density difference (CDD) plots in Figure 4a, which show the redistribution of charge induced by the different bond structures (details provided in the Supporting Information). Close to the dopant center, there are substantial local changes in the charge, including bond polarization effects. Further from the dopant center, an increase in charge density of the carbon π-network is uniquely observed for the N3 dopant; N1 and N2 groups and vacancy defects on the other hand withdraw charge from the π-orbitals (see Supporting Information Figure S5).

The different N-bond environments not only result in a clear signature in the N 1s XAS spectra, but at the present doping levels, they can also clearly influence the C 1s XAS and XES spectra (Figure 4b). Figure 4b compares C 1s XES and XAS for pristine ($PG2/SiO_2$) and N-doped ($NG2/SiO_2$) graphene transferred to SiO_2 (XPS shown in Figure 2a) in which N1, N2 (p-type), and N3 (n-type) dopants coexist (see Figure 3 and Supporting Information Figure S3). Estimates of the concentration of N1, N2, and N3 dopants in $NG2/SiO_2$ from XPS are provided in Supporting Information Figure S4. Angle-dependent C 1s XAS shows that the transferred samples are significantly rippled compared to graphene grown directly on Cu foil (see Supporting Information Figure S5). The deviation from planarity, an expected consequence of lithographic transfer methods,[36] results in a mixing of σ and π signals in the XES emission channels and polarization-dependent XAS. The in-plane XAS and normal emission XES are nonetheless dominated by σ-states, while the out-of-plane XAS (and corresponding XES) are dominated by π-states. We also note the presence of small concentrations (~0.1%) of N1 and N2 dopant structures observed in $PG2/SiO_2$ with XPS (see Supporting Information Figure S9). This will act to reduce the spectral differences observed between samples $PG2/SiO_2$ and $NG2/SiO_2$ induced by N1 and N2 type dopants, nonetheless N1 and N2 bond signatures in sample $NG2/SiO_2$ are still evident.

Distinct features in the C 1s XES and XAS, labeled 1–6 in Figure 4b, are observed for $NG2/SiO_2$ relative to $PG2/SiO_2$. These features reflect the interplay of dopant-induced changes to the electronic structure, which are represented schematically in Figure 4c based on computed pDOS and simulated XES for

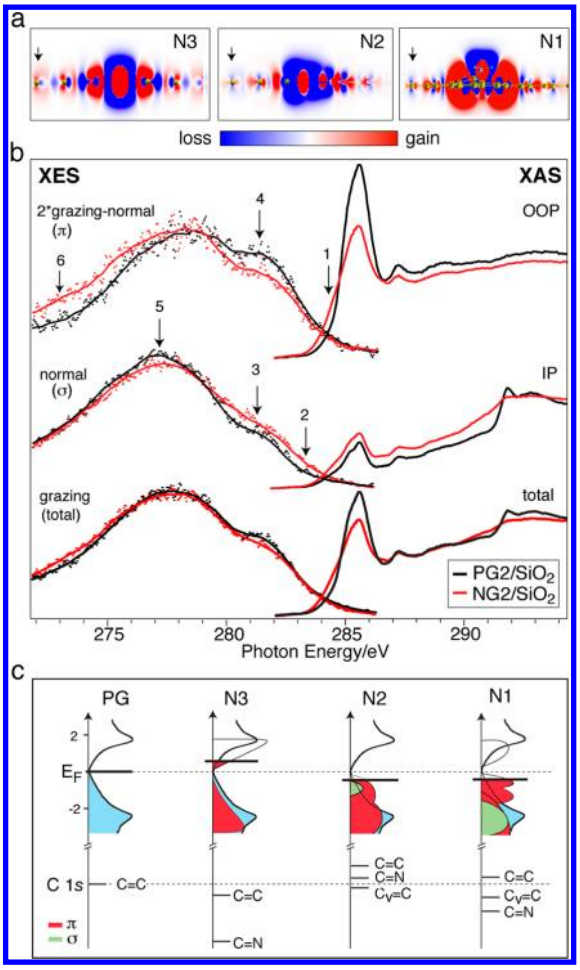

Figure 4. (a) Charge density difference (CDD) plots for a single N3 (left), N2 (center), and N1-type (right) dopant. The plots show the gain (red) and loss (blue) of charge in the C π-network for the n- (N3) and p-type (N2 and N1) dopants, respectively; arrows are drawn to guide the eye. The CDD is taken relative to pristine graphene (PG) in the N3 case ($\rho_{diff} = \rho(NG) - \rho(PG)$) and relative to PG with vacancy (CDD shown in Supporting Information Figure S5) defect(s) in the N2 and N1 cases ($\rho_{diff} = \rho(NG) - \rho(PG_{vac})$) where PG_{vac} indicates pristine graphene with a vacancy. (b) C 1s symmetry-resolved XES (left) and in- (IP) and out-of-plane (OOP) XAS (right) for pristine ($PG2/SiO_2$) and N-doped graphene ($NG2/SiO_2$) transferred to SiO_2 for which XPS is shown in Figure 2. Note that the buckling on the SiO_2 generates a significant π and σ mixing in both XAS and XES; total (bottom), σ-dominated (center), and π-dominated (top) spectra are shown (see text). The XAS data is normalized by area past the continuum (330 eV). (c) Schematic of the π-band structure of PG (black curve, blue fill for occupied states, white for unoccupied) and distinct C 1s core and Fermi level shifts and new states (red and green fill correspond to the sum of occupied π- and σ-states, respectively, for the carbon atoms in the vicinity of the N-dopant) based on computed pDOS and simulated XES provided in the Supporting Information. C═N, C═C, and C_v═C signify the carbon bonded to the N-dopant, the next-nearest neighbor, and to the C atom at a vacancy site (N2 and N1), respectively. Specific values for the shifts are listed in the Supporting Information.

graphene doped at the 1% level (Supporting Information Figures S7 and S8). First, there is an overall shift of the Fermi level with doping (see Table 1). Second, the C atoms that are near the point defects have a shift in the local 1s level and a change in the local density of states due to interactions with the N centered region. Since XAS and XES spectra result from

dx.doi.org/10.1021/nl301409h | Nano Lett. 2012, 12, 4025–4031

atom-localized absorption or emission events, these sites make distinct contributions to the spectra that are in aggregate clearly detectable.

The N-induced changes in the π-dominated XES/XAS data (Figure 4b top) are well represented by band structure differences between N3-doped graphene relative to PG (Figure 4c), suggesting that graphitic dopants dominate this channel. Specifically, we observe a suppression of π-states, particularly around the peak in the density of states below the Fermi level E_F resulting in the suppression of intensity in the 280−282 eV range (feature 4 in Figure 4b top). The calculations also indicate a shift of the center of π-states near the N3 dopant to higher BE (lower photon energy), and development of a significant peak in the local density of states at the bottom of the π band (∼9 eV below E_F, see Supporting Information Figure S7). These changes induced by the N3 dopant lead to the increase of intensity in the XES below 278 eV (feature 6 in Figure 4b top). Moreover, a shoulder appears on the low energy side of the π^* resonance at 285.5 eV of the NG2/SiO_2 XAS (feature 1 in Figure 4b top); we note that a corresponding shoulder appears on the low BE side of the C 1s photoemission for this sample (Figure 2b). This shoulder results primarily from partially unoccupied carbon π-states due to N3, see Figure 4c. This is consistent with a recent report by Schultz et al.[36] in which the pre-edge shoulder on the C═C π^* resonance was attributed to doping, rather than to vacancy or edge defects[37] and shown to be independent of the degree of corrugation in the transferred layer, which shifts the graphene Dirac point. We note that carbon atoms at vacancy defects (with or without N present) may contribute to this shoulder, although to a much lesser degree (see, e.g., N1 in Figure 4c and Supporting Information Figure S7). (The simulated spectra for N1 and N2 dopants show a similar suppression, as well as a modest enhancement in the 282−284 eV range (Supporting Information Figure S8) that is not observed in the high energy tail of the XES.)

On the other hand, the changes in the normal emission (σ-dominated) XES for NG2/SiO_2 relative to PG2/SiO_2 are largely represented by the electronic effects of the N2 and N1 dopants. All three dopants show a suppression of σ local density of states in the range 5−7 eV below the Fermi energy and an overall redistribution of the density of states to lower energy (Supporting Information Figure S7), which contributes to the reduced intensity around 278 eV (feature 5 in Figure 4b middle). However, N2 and N1 dopants introduce states with σ character close to the Fermi energy (Figure 4c and Supporting Information Figure S7), which correspond to features 2 and 3 in Figure 4b, center; the simulated XES clearly shows added intensity around 282 and 280 eV for N2 and N1 respectively in the normal emission signal (Supporting Information Figure S8). N2 and N1 (without hydrogen) introduce occupied nonbonding (lone-pair) σ-states, while the hydrogenated N1 dopants (Figure 3) introduce occupied N−H σ-states (see pDOS in Supporting Information Figure S7). Interestingly, simulations show that the isolated vacancy introduces additional intensity near 283 eV (Supporting Information Figure S8), which may also contribute to the significant enhancement of intensity observed in the high energy tail of the normal emission XES (Figure 4b middle).

In addition to distinct E_F shifts for the different N-dopant bond structures (Table 1), the C 1s level of the carbon atom bonded to the N-dopant and that of the next-nearest neighbor (C═C) are also sensitive to the details of the N-bond environment and significant variation in the magnitude and direction of the shift is observed across the N-dopant bond series (values provided in Supporting Information). The C 1s level of the carbon atom at a vacancy (C_v═C) shifts (by different amounts) to higher BE for the N2 and N1-type dopants (Figure 4c); interestingly, the opposite shift is observed for a carbon atom at vacancy site in pristine graphene. (The calculations indicate that the electronic structure of graphene is only perturbed in the close proximity (first two coordination shells) of the N-dopant, as visualized in Figure 4a and consistent with our previous findings for individual N3-dopants.[13]) The broader energy distribution of the occupied π- and σ-states (∼0−6 eV relative to E_F), as well as the distinct core-level and E_F shifts for N1, N2, and N3 dopants (Table 1 and Figure 4c), account for the width of the shoulder in the measured XES, while the partially unoccupied π-states produce the XAS shoulder.

The observed electronic effect of the different bond structures in N-doped graphene can be understood in a simple chemical bond picture, summarized in the following. In the N3-case, four of the five valence electrons in N fill the σ- and π-orbitals as for C, leaving one extra electron. The additional charge is to ∼50% localized on the N3 dopant, which electronically couples to its nearest C neighbors. Consequently we observe a single N nonbonding π-orbital resonance in the projected density of states (pDOS)[13] and in the simulated XES (Supporting Information) at the Fermi energy, and a largely unoccupied p_z state on the N3-bonded carbon (Figure 4c). The remaining charge of ∼0.5 electron per N3 dopant is distributed in the local network of carbon π-states and n-dopes the system;[13] this appears as a gain in orbital occupation (pDOS) and charge density of the π-orbitals (Figure 4a left). In contrast, N2 and N1 dopants have the opposite electronic effect; they withdraw charge from the carbon π-network (Table 1 and Figure 4a) to p-dope graphene. In the N2-case, two electrons fill σ-bonds with carbon neighbors, two electrons form a lone pair in the graphene plane, and the remaining electron occupies the N π-state (Figure 4c and Supporting Information). Thus, the N2 dopant has the equivalent occupation of a nominal carbon in graphene, but a π-electron is missing due to the vacancy site so the system is p-doped. Similarly, the N1 dopant forms one σ-bond with its C neighbor, forms σ-bonds to two H (or one N-lone-pair orbital in the unhydrogenated case). Two electrons go into the π-network, but as for the N2 case, the missing π-electrons from the divacancy sites that accommodate this form of the N dopant result in overall p-type doping, which is further enhanced by the polarization of charge in the plane of the N-dopant (see Figure 4a center). In contrast, if the conditions for the formation of the lone-pairs or other localized states (like edge states) are unfavorable, for example, in the graphitic case or hydrogenated pyridinic groups (Table 1), the additional charge from nitrogen is forced to go to the extended carbon π-network, essentially neutralizing the p-doping effect in the N2 case (Table 1).

In summary, we have presented a microscopic understanding of the different bond types and their diverse effects on the workfunction, carrier concentration and the local electronic structure in nitrogen-doped graphene films from core-level spectroscopy and DFT. These findings show that controlling the bonding-type of dopant substitutions in graphene is essential when designing properties of graphene as functional component in future devices. This work demonstrates that synchrotron radiation based spectroscopies provide invaluable,

dx.doi.org/10.1021/nl301409h | Nano Lett. 2012, 12, 4025−4031

atom-specific tools to determine the resulting electronic properties of different dopant and defect structures in graphene, even at subpercent dopant levels. Combined with continuing advances in the growth, controlled doping of graphene, and cleaner transfer procedures, the detailed correlation of bond type and electronic structure demonstrated here promises to facilitate the atomic-level control of electronic properties desired for next generation graphene-based devices.

■ ASSOCIATED CONTENT

Supporting Information

Experimental and theoretical details, including cluster models. Additional characterization of pristine and N-doped graphene transferred to SiO_2, including C 1s and N 1s XPS, XAS, and workfunction measurements; computed XES and pDOS are also provided. This material is available free of charge via the Internet at http://pubs.acs.org.

■ AUTHOR INFORMATION

Corresponding Author

*E-mail: (T.S.) ts2526@columbia.edu; (A.N.P.) apn2108@columbia.edu.

Notes

The authors declare no competing financial interest.

■ ACKNOWLEDGMENTS

Research supported by the EFRC Center for Re-Defining Photovoltaic Efficiency through Molecule Scale Control (award DE-SC0001085). Portions of this research were carried out at beamlines 11-3 and 13-2 at the Stanford Synchrotron Radiation Laboratory, a national user facility operated by Stanford University on behalf of the U.S. Department of Energy, Office of Basic Energy Sciences, and at the Center for Functional Nanomaterials, and beamlines X-9 and U7A at the National Synchrotron Light Source, Brookhaven National Laboratory, which are supported by the U.S. Department of Energy, Office of Basic Energy Sciences, under Contract No. DE-AC02-98CH10886. Support also provided by AFOSR under Grant FA9550-11-1-0010 (A.N.P), for research carried out in part at the Center for Functional Nanomaterials, Brookhaven National Laboratory, Contract No. DE-AC02-98CH10886 (M.S.H.), and at the National Synchrotron Light Source, Contract No. DE-AC02-98CH10886, by ONR under Graphene MURI (A.P. and P.K.), by NSF under Grant CHE-0641523 (A.P.), by NYSTAR, and by Priority Research Centers Program (2012-0005859), Basic Science Program (2011-0029645) through the National Research Foundation of Korea (NRF) funded by the Ministry of Education, Science, and Technology (K.S.K). L.G.M.P. acknowledges support from the EU FP7 HYPOMAP network.

■ REFERENCES

(1) Nair, R. R.; Blake, P.; Grigorenko, A. N.; Novoselov, K. S.; Booth, T. J.; Stauber, T.; Peres, N. M. R.; Geim, A. K. Fine Structure Constant Defines Visual Transparency of Graphene. *Science* **2008**, *320*, 1308.

(2) Ohta, T.; Bostwick, A.; Seyller, T.; Horn, K.; Rotenburg, E. Controlling the Electronic Structure of Bilayer Graphene. *Science* **2006**, *313*, 951.

(3) Yu, Y.-J.; Zhao, Y.; Ryu, S.; Brus, L. E.; Kim, K. S.; Kim, P. Tuning the Graphene Work Function by Electric Field Effect. *Nano Lett.* **2009**, *9* (10), 3430−3434.

(4) Cox, M.; Gorodetsky, A.; Kim, B.; Kim, K. S.; Jia, Z.; Kim, P.; Nuckolls, C.; Kymissis, I. Single-layer graphene cathodes for organic photovoltaics. *App. Phys. Lett.* **2011**, *98*, 123303.

(5) Wang, Y.; Shao, Y.; Matson, D. W.; Li, U.; Lin, Y. Nitrogen-Doped Graphene and Its Application in Electrochemical Biosensing. *ACS Nano* **2010**, *4* (4), 1790−1798.

(6) Wang, X.; Li, X.; Zhang, L.; Yoon, Y.; Weber, P.; Wang, H.; Guo, J.; Dai, H. N-doping of graphene through electrothermal reactions with ammonia. *Science* **2009**, *324* (5928), 768−771.

(7) Guo, B.; Liu, Q.; Chen, E.; Zhu, H.; Fang, L.; Gong, J. R. Controllable N-doping of graphene. *Nano Lett.* **2010**, *10*, 4975−4980.

(8) Choi, J.; Lee, H.; Kim, K.-J.; Kim, B; Kim, S. Chemical Doping of Epitaxial Graphene by Organic Free Radicals. *J. Phys. Chem. Lett.* **2010**, *1*, 505−509.

(9) Li, X.; Wang, H.; Robinson, J. T.; Sanchez, H.; Diankov, G.; Dai, H. Simultaneous Nitrogen Doping and Reduction of Graphene Oxide. *J. Am. Chem. Soc.* **2009**, *131* (43), 15939−15944.

(10) Wei, D.; Liu, Y.; Wang, Y.; Zhang, H.; Huang, L.; Yu, G. Synthesis of N-doped Graphene by Chemical Vapor Deposition and Its Electrical Properties. *Nano Lett.* **2009**, *9* (5), 1752−1758.

(11) Abbas, G.; Papakonstantinou, P.; Iyer, G. R. S.; Kirkman, I. W.; Chen, L. C. Substitutional nitrogen incorporation through rf glow discharge treatment and subsequent oxygen uptake on vertically aligned carbon nanotubes. *Phys. Rev. B* **2007**, *75* (19), 195429.

(12) Lee, V.; Whittaker, L.; Jaye, C.; Baroudit, K. M.; Fischer, D. A.; Banerjee, S. Large-Area Chemically Modified Graphene Films: Electrophoretic Deposition and Characterization by Soft X-ray Absorption Spectroscopy. *Chem. Mater.* **2009**, *21* (16), 3905−3916.

(13) Zhao, L.; He, R.; Rim, K. T.; Schiros, T.; Kim, K. S.; Zhou, H.; Kim, K. S.; Zhou, H.; Gutiérrez, C.; Chockalingam, S. P.; Arguello, C. J.; Pálová, L.; Nordlund, D.; Hybertsen, M. S.; Reichman, D. R.; Heinz, T. F.; Kim, P.; Pinczuk, A.; Flynn, G. W.; Pasupathy, A. N. Visualizing individual nitrogen dopants in monolayer graphene. *Science* **2011**, *333*, 999−1003.

(14) Usachov, D.; Vilkov, O.; Grüneis, A.; Haberer, D.; Fedorov, A.; Adamchuk, V. K.; Preobrajenski, A. B.; Dudin, P.; Barinov, A.; Oehzelt, M.; Laubschat, C.; Vyalikh, D. V. *Nano Lett.* **2011**, *11* (12), 5401−5407.

(15) Panchakarla, L. S.; Subrahmanyam, K. S.; Saha, S. K.; Govindaraj, A.; Krishnamurthy, H. R.; Waghmare, U. V.; Rao, C. N. R. Synthesis, structure, and properties of boron- and nitrogen-doped graphene. *Adv. Mater.* **2009**, *21* (46), 4726−4730.

(16) Hanafusa, A.; Muramatsu, Y.; Kaburagi, Y.; Yoshida, A.; Hishiyama, Y.; Yang, W.; Denlinger, J. D.; Gullikson, E. M. Local structure analysis of boron-doped graphite by soft x-ray emission and absorption spectroscopy using synchrotron radiation. *J. Appl. Phys.* **2011**, *110*, 053504.

(17) Walter, A.; Jeon, K.-J; Bostwick, A; Speck, F; Ostler, M.; Seyller, T.; Moreschini, L.; Kim, Y. S.; Chang, Y. J.; Horn, K.; Rotenberg, E. Highly p-doped epitaxial graphene obtained by fluorine intercalation. *App. Phys. Lett.* **2011**, *98*, 184102.

(18) Ryu, S.; Han, M. Y.; Maultzsch, J.; Heinz, T. F.; Kim, P.; Steigerwald, M. L.; Brus, L. E. Reversible Basal Plane Hydrogenation of Graphene. *Nano Lett* **2008**, *8*, 4597−602.

(19) Stöhr, J. *NEXAFS spectroscopy*; Springer-Verlag: New York, 1992.

(20) Brühwiler, P. A; Maxwell, A. J.; Puglia, C; Nilsson, A.; Andersson, S.; Mårtensson, N. π^* and σ^* Excitons in C 1s Absorption of Graphite. *Phys. Rev. Lett.* **1995**, *74* (4), 614−617.

(21) I. Shimoyama, I.; Wu, G.; Sekiguchi, T.; Baba, Y. Evidence for the existence of nitrogen-substituted graphite structure by polarization dependence of near-edge x-ray-absorption fine structure. *Phys. Rev. B* **2000**, *62*, 6053−6.

(22) Hellgren, N.; Guo, J.; Luo, Y.; Såthe, C.; Agui, A.; Kashtanov, S.; Nordgren, J.; Ågren, H.; Sundgren, J.-E. Electronic structure of carbon nitride thin films studied by X-ray spectroscopy techniques. *Thin Solid Films* **2005**, *471* (1−2), 19−34.

(23) Hellgren, N.; Guo, J.; Luo, Y.; Såthe, C.; Agui, A.; Kashtanov, S.; Nordgren, J.; Ågren, H.; Sundgren, J.-E. Nitrogen bonding structure in

carbon nitride thin films studied by soft x-ray spectroscopy. *App. Phys. Lett.* **2001**, *79* (26), 4348−50.
(24) Jiménez, I.; Gago, R.; Albella, J. M.; Cáceres, D.; Vergara, I. Spectroscopy of π bonding in hard graphitic carbon nitride films: Superstructure of basal planes and hardening mechanisms. *Phys. Rev. B* **2000**, *62* (7), 4261−4264.
(25) Triguero, L.; Pettersson, L. G. M.; Ågren, H. Calculations of Near-Edge X-ray Absorption Spectra of Gas Phase and Chemisorbed Molecules by means of Density Functional and Transition Potential Theory. *Phys. Rev. B* **1998**, *58*, 8097.
(26) Hermann, K.; Pettersson, L. G. M.; Casida, M. E.; Daul, C.; Goursot, A.; Koester, A.; Proynov, E.; St-Amant, A.; Salahub, D. R.; Carravetta, V.; Duarte, A.; Godbout, N.; Guan, J.; Jamorski, C.; Leboeuf, M.; Leetmaa, M.; Nyberg, M.; Pedocchi, L.; Sim, F.; Triguero, L.; Vela, A. *StoBe-deMon*, 5.3 ed.; StoBe-deMon Software: Stockholm-Berlin, 2005.
(27) Lin, Y. C.; Lin, C. Y.; Chiu, P. W. Controllable graphene N-doping with ammonia plasma. *App. Phys. Lett.* **2010**, *96* (13), 133110.
(28) Point, S.; Minea, T.; Bouchet-Fabre, B.; Granier, A.; Turban, G. XPS and NEXAFS characterisation of plasma deposited vertically aligned N-doped MWCNT. *Diamond Relat. Mater.* **2005**, *14* (3−7), 891−895.
(29) (a) Yeh, J.-J.; Lindau, I. Atomic Subshell Photoionization Cross Sections and Asymmetry Parameters: $1 < Z < 103$. *At. Data Nucl. Data Tables* **1985**, *32*, 1. (b) Yeh, J.-J. *Atomic Calculations of Photoionization Cross Sections and Asymmetry Parameters*; Gordon and Breach: Langhorne, PA, 1993.
(30) The atomic N concentration can be estimated from the ratio of N 1s and C 1s XPS intensity, normalized by the respective ionization cross-sections for carbon and nitrogen at a given kinetic energy. Here excitation energies of 400 and 520 eV were used for the carbon and nitrogen XPS, respectively, to eject photoelectrons with ∼120 eV kinetic energy.
(31) Reddy, A. L.; Srivastava, A.; Gowda, S. R.; Gullapalli, H.; Dubey, M.; Ajayan, P. M. Synthesis Of Nitrogen-Doped Graphene Films For Lithium Battery Application. *ACS Nano* **2010**, *4* (11), 6337−6342.
(32) Sheng, Z.-H.; Shao, L.; Chen, J. −J.; Bao, W. −J.; Wang, F. −B.; Xia, X. -H. Catalyst-Free Synthesis of Nitrogen-Doped Graphene via Thermal Annealing Graphite Oxide with Melamine and Its Excellent Electrocatalysis. *ACS Nano* **2011**, *5* (6), 4350−4358.
(33) Casanovas, J.; Ricart, J. M.; Rubio, J.; Illas, F.; Jiménez-Mateos, J. M. Origin of the Large N 1s Binding Energy in X-ray Photoelectron Spectra of Calcined Carbonaceous Materials. *J. Am. Chem. Soc.* **1996**, *118*, 8071−8076.
(34) A. Nilsson, A.; Zdansky, E.; Tillborg, H.; Björneholm, O.; Mårtensson, N.; Andersen, J. N.; Nyholm, R. Photoabsorption and the Unoccupied Partial Density of States of Chemisorbed Molecules: CO on Ni(100). *Chem. Phys. Lett.* **1992**, *197*, 12.
(35) Giannozzi, P.; et al. Quantum Espresso: a modular and open-source software project for quantum simulations of materials. *J. Phys.: Condens. Matter* **2009**, *21*, 395502.
(36) Schultz, B.; Patridge, C. J.; Lee, V.; Jaye, C.; Lysaght, P. S.; Smith, C.; Barnett, J.; Fischer, D. A.; Prendergast, D.; Banerjee, S. Imaging local electronic corrugations and doped regions in graphene. *Nat. Commun.* **2011**, *2*, 372.
(37) Hua, W.; Gao, B.; Li, S.; Ågren, H.; Luo, Y. X-ray absorption spectra of graphene from first-principles simulations. *Phys. Rev. B* **2010**, *82* (15), 155433.